Raman study of insulating and conductive ZnO:(Al, Mn) thin films

M. F. Cerqueira[a], T. Viseu[a], J. Ayres de Campos[a], A. G. Rolo[a], T. de Lacerda-Aroso[a], F. Oliveira[a], I. Bogdanovic-Radovic[b], E. Alves[c], M. I. Vasilevskiy[a]

[a] Centro de Física e Departamento de Física, Universidade do Minho, Campus de Gualtar, 4710-057 Braga, Portugal
[b]RudjerBoskovicInstitute, Bijenicka cesta 54, 10000 Zagreb, Croatia
[c]Instituto de Plasmas e Fusão Nuclear, Instituto Superior Técnico, Universidade Técnica de Lisboa, EN10, 2696-953 Sacavém, Portugal

Abstract

Raman spectroscopy results obtained for undoped and Al- and/or Mn-doped ZnO thin films produced by RF-sputtering are reported. The effect of the doping method (either co-sputtering or ion implantation), the dopant type and its concentration on the Raman-active vibrational modes in these films were studied in detail. The results are discussed with focus on the peak shifts and broadening, and on the doping-induced relaxation of the symmetry selection rules. A particular attention is paid to the 520-530 cm^{-1} Raman band observed in all Mn containing samples and a simple theoretical model and arguments are presented in support of its relation to the local (gap) phonon mode produced by Mn atoms substituting Zn in the cationic sublattice of the ZnO crystal.

1. Introduction

Transparent conducting oxides (TCOs) have long been the subject of numerous studies due to their unique physical properties and device applications [1-3]. Zinc oxide (ZnO) is a particularly interesting TCO example. Pure ZnO is a natural *n*-type semiconductor because of the presence of intrinsic oxygen vacancies and/or interstitial zinc atoms [4]. Its electrical properties can be improved by doping with IIIA-group elements, like Al, achieving lower resistivity values [5] although keeping its desired optical properties, namely the transparency. On the other hand, dilute magnetic semiconductors (DMS) have also recently attracted much attention for their promising functionalities in spintronics due to their properties involving electron spin. To take advantage of both charge and spin of electrons in semiconductors, magnetic elements can be introduced in the nonmagnetic III-V semiconductors currently used in optoelectronic devices [6]. However, incorporation of these magnetic elements for obtaining robust spin polarization in existing semiconductors is not a straightforward technology because

there are still some technical issues to be overcome [7], even though this possibility is still promising. Particular attention has been devoted to ZnO-based DMS materials that had been predicted to be ferromagnetic at room temperature [8-10]. Nevertheless, experimentally they were found to have lower magnetic ordering temperatures [11, 12] or no ferromagnetism at all, at least above 4K [13, 14], even though communications of room-temperature ferromagnetic behavior of ZnO:Mn with a high Curie temperature appear in the literature from time to time [15]. It has been suggested that surface and grain boundaries may be more important for the magnetic properties of DMS than doping with magnetic ions itself [16]. These controversial results imply that magnetism, as well as the conductivity, is very sensitive to the morphology and structure of the samples and the way the impurities are incorporated into the crystal lattice. Of course, all these issues are related to the method of preparation of the material.

In this study, the doping elements are Al (donor impurity) and Mn (magnetic impurity) and they have been incorporated in the ZnO lattice by either co-sputtering or ion implantation. The work is focused on the modification of the vibrational modes of ZnO lattice caused by the doping with Al and Mn in different concentrations and performed by different methods. A better understanding of the electronic and lattice properties of doped ZnO layers, in particular of how these properties depend on the way the dopant is incorporated into the ZnO lattice, is a fundamental requirement to improve the quality and performance of the devices. As expected, films doped with Al become conductive. As shown in Table 1, the conductivity is even preserved for RF sputtered ZnO:Al *a posteriori* implanted with Mn ions.

All samples were studied by Raman spectroscopy, the principal experimental technique in this work. The results are correlated with the doping method and the impurity concentration analyzing their effect on the characteristic vibrational modes of these materials. Non-resonant excitation with the energy of incident photons below the band gap energy of ZnO (E_g = 3.37 eV) was chosen because resonant Raman spectra are dominated by the LO-phonon line and its replicas, which are strongly enhanced by the Fröhlich interaction with real (not virtual) electron-hole pairs [17]. In contrast, Raman lines due to local impurity modes and non-polar vibrations, the ones important in this study, are not enhanced in the same way under interband resonance conditions. An extended discussion of the nature of a Raman band located at 520-530 cm^{-1} and observed in all Mn containing samples, as strong as the principal ZnO phonon features under non-resonant conditions, is presented.

2. Growth and characterization details

ZnO thin films were grown on glass substrates in an Alcatel SCM 650 sputtering system, within a mixture of O_2 and Ar gases, at a constant working pressure (10^{-3} mbar). The target consisted of a hyper-pure (99.99%) metal zinc wafer spaced 60 mm away from the substrates. Radio frequency (13.56 MHz) reactive sputter deposition was carried out after the chamber had reached a base pressure near 10^{-6} mbar. The deposition rate was approximately 2 nm/min and the grown layers had a sub-micrometer thickness (see Table 1).

Three groups of samples were prepared. The first group comprises sputtered ZnO thin films doped by implantation with different contents of Al or Mn ions. A high flux ion implanter (Danfysic model S1090) was used with an implantation energy of 100 keV and fluencies ranging from 1×10^{15} to 10×10^{15} atoms.cm^{-2}. The second group includes ZnO doped thin films prepared by co-sputtering placing small pieces of Al or/and Mn (both 99.99% pure) above the Zn target. A third group of samples consists of co-sputtered ZnO:Al thin films *a posteriori* implanted with Mn ions. All samples were then annealed at 500^{o}C for 60 min in air at atmosphere pressure.

For the ion implantation energy used, the implantation profile is centered at about 50 nm from the sample surface as revealed by ion beam analysis and determined by SRIM [18]**,** much lower than the sample thickness. In order to verify if the *pos*-annealing treatment carried out was efficient to spread the Mn ions into the ZnO thin film, a gradual etching of the sample surface, with diluted hydrochloric acid (3% HCl in deionized water at room temperature), has been done. After removing at least 350 nm the presence of the Mn ions is still observed by Raman spectroscopy. This means that Mn ions diffuse over a much larger distance than that corresponding to the effective implantation depth.

The composition of the films was determined by TOF-ERDA (time-of-flight elastic recoil detection analysis). These measurements were done at the Ruđer Bošković Institute in Zagreb using 25.5 MeV iodine ions. The beam current during the measurement was ~ 3 nA. Detector was placed at 37.5° and the angle between beam and sample surface during the measurements was 20°.

The electric resistivity was measured at room temperature in a standard dc system using the Van der Pauw technique. The thickness and optical parameters of the films were determined by optical transmittance measurements in the UV-vis-NIR range (300 -

2500 nm), using a Shimadzu UV-3101-PC spectrophotometer. The micro-structure of the films was analyzed by means of X-ray diffraction and micro-Raman scattering. X-ray experiments were performed at room temperature in a Philips PW 1710 diffractometer using Cu-K_α radiation, in a Bragg-Bretano geometry, in the range $10^o < 2\theta < 80^o$. Room temperature micro-Raman spectra were measured on a Jobin-Yvon T64000 spectrometer equipped with a liquid nitrogen cooled CCD detector, in a frequency range of 200-780 cm^{-1}, using the 514.5 nm excitation line of an Ar^+ laser, with an incident power of 4 mW in a 1 μm spot and backscattering geometry.

3. Experimental results and discussion

3.1 – General characterization and structure

All the ZnO thin films produced, undoped and doped, are highly transparent and polycrystalline. Fitting the transmission spectra, by using the Minkov method [19] and a classical Lorentz function for the dispersion of the ZnO dielectric function, the thickness and the optical parameters of the films were obtained. A typical transmission spectrum and the corresponding fit are shown in figure 1(a).

Table 1 *– Relevant characterization parameters of the analyzed samples*

Sample number	Preparation method*	Al (at.%)	Mn (at.%)	Thickness (nm)	Crystalline size (nm)	ρ (Ω cm)
#1	ZnO(sp)	—	—	625	25.5	$> 2\times10^8$
#2	ZnO(sp):Al(sp)	0.5	—	780	20.0	≈ 0.05
#3	ZnO(sp):Al(imp)	< 0.5	—	350	21.3	≈ 0.1
#4	ZnO(sp):Mn(sp)	—	0.4	1040	18.4	$> 2\times10^8$
#5		—	1.1	830	11.8	$> 2\times10^8$
#6	ZnO(sp):Mn(imp)	—	1.1	515	18.4	$> 2\times10^8$
#7		—	3.3	515	20.5	$> 2\times10^8$
#8		—	5.3	515	20.5	$> 2\times10^8$
#9	ZnO(sp):Al(sp):Mn(imp)	0.5	1.5	780	19.0	≈ 0.05
#10		0.5	2.2	780	20.5	≈ 0.05
#11	ZnO(sp):Al(sp):Mn(sp)	1.1	1.6	412	11.8	$> 2\times10^8$

* (sp) *stands for sputtering and* (imp) *means ion implantation*

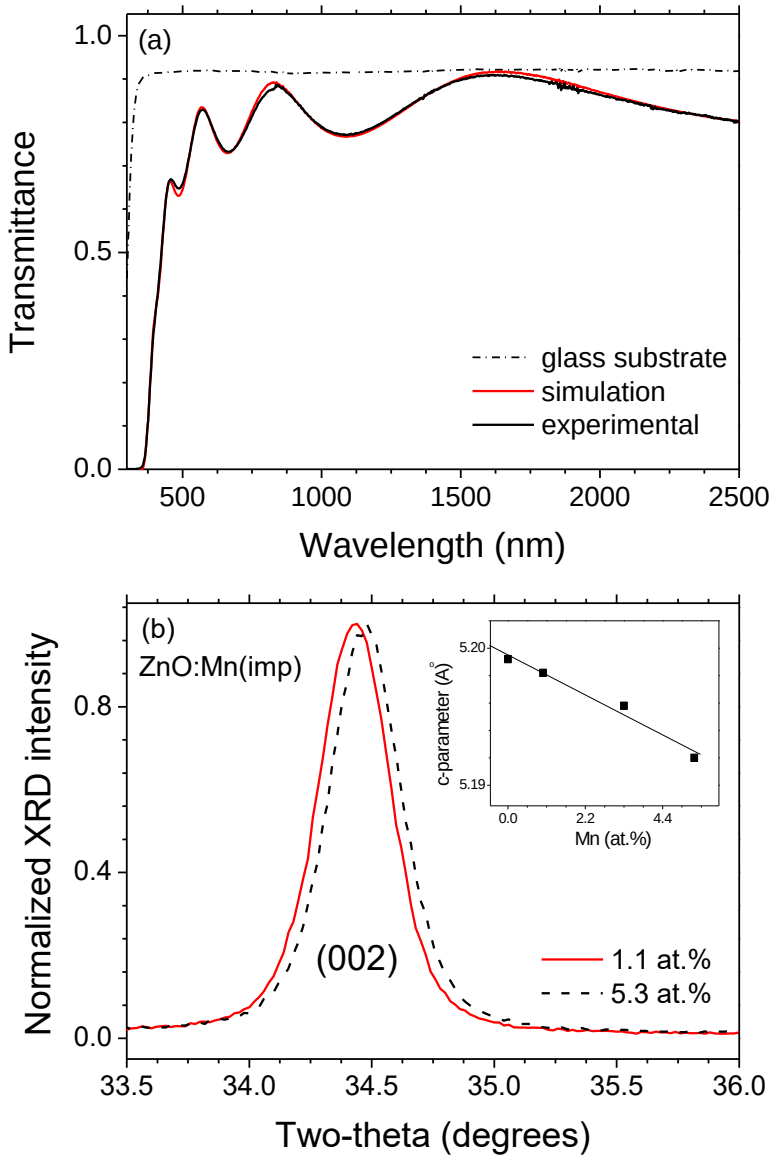

Figure 1. *a) Transmittance spectrum and the corresponding fit for sample (ZnO doped with Al and Mn ions by co-sputtering). The spectrum of glass substrate is also shown for comparison. b) XRD patterns, in the (002) Bragg reflection peak region, of two Mn implanted ZnO samples showing the effect of the increase in Mn content. Inset: c-parameter of ZnO lattice as a function of the Mn content.*

According to X-ray diffraction results, the micro-crystallites have a wurtzite structure and show a strongly preferential orientation with the *c*-axis perpendicular to the substrate surface, independent of the doping method and concentration. Figure 1(b) shows typical X-ray diffractograms in the region of the (002) peak for two ZnO:Mn implanted samples. In the inset, the impact of the Mn doping on the ZnO lattice is shown by the dependence of the *c*-parameter on Mn content. We assume that hydrostatic strain in our films is relaxed because they are polycrystalline. The observed decrease of

the *c*-parameter as the Mn concentration increases is in agreement with the behaviour observed for low Mn content [20, 21], where it was verified that only above a certain threshold the *c*-parameter starts to increase with the growth of the Mn content. The average domain size (D) was calculated analyzing the (002) peak, according the Scherer procedure described in the literature [22] and the results are presented in Table 1. The contents of Al or/and Mn, obtained by TOF-ERDA are also given in Table 1.

3.2 – Electrical properties

The electrical resistivity (ρ) of the films was measured using the Van der Pauw method and the results are presented in Table1. As expected, nominally pure ZnO thin films are highly resistive. In contrast, all Al doped films are conductive, either those prepared by co-sputtering (sample#2) or the implanted ones (sample #3). However, the incorporation of very small amounts of Mn by co-sputtering (samples #4 and #5) or by implantation (samples #6, #7 and #8), greatly increases the resistivity of the samples. However, samples doped with both ions exhibit different behaviors depending on the doping method. If Mn is implanted into a conductive ZnO:Al(sp) film, it remains conductive (samples #9 and #10), nevertheless if Mn and Al are simultaneously co-sputtered, samples are highly insulating (sample #11). This effect was also observed in other Al-Mn co-sputtered samples (not shown in this paper).

These results seem to indicate that, if Al ions are previously incorporated in the ZnO crystal lattice, mainly occupying Zn sites and acting as shallow donors [23], the subsequent implantation of Mn ions does not strongly modify the lattice and so the films remain conductive. In contrast, the co-sputtered samples are highly resistive (more than five orders of magnitude higher!) which seems to indicate that, when both ions are simultaneously incorporated, Al ions are not able to replace properly Zn atoms in the lattice.This huge difference in the conductivity of these two sets of ZnO:Al:Mn samples, is too large to be attributed just to a decrease in the electron mobility due to additional lattice defects.

3.3 Raman spectroscopy

3.3.1 – Undoped ZnO

The wurtzite-type lattice structure of ZnO implies a basic unit of four atoms ($n = 4$) in the unit cell (two Zn-O molecular units), then the number of phonon modes amounts to $3n = 12$, being three acoustic (one longitudinal, LA, and two transverse, TA) and nine

optical phonons (three longitudinal, LO, and six transverse, TO). At the Γ-point of the Brillouin zone, the optical phonons have the following irreducible representations: $\Gamma_{opt}=A_1+2B_1+E_1+2E_2$ [24] (the E modes are twofold degenerate). The B_1 modes are silent, i.e. both IR and Raman inactive, and the E_2vibrations are only Raman active (non-polar). The Raman and IR active phonons A_1 and E_1 are polar and therefore each of them splits into LO and TO modes with different frequencies due to the macroscopic electric field of the LO phonons. Note that it does not mean an increase of the total number of modes because *exactly* in the Γ-point the LO and TO modes remain degenerate since the electric field vanishes at infinity and for any small but finite wavevector only three A_1+E_1 modes exist. For instance, for $\vec{q}$ parallel to the *c*-axis one has the A_1(LO) and (double degenerate) E_1(TO) modes, while for $\vec{q}$ perpendicular to the *c*-axis the two TO modes correspond to different representations, A_1+E_1. The TO-LO splitting is considerably larger than the anisotropy-related A_1 - E_1 separation [25]. The (near) zone-center optical phonon frequencies lie between approximately 100 cm^{-1} and 600 cm^{-1}.

The Raman scattering cross-section of the LO phonon modes is determined by both optical deformation potential (ODP) and Fröhlich electron-phonon interaction. The Fröhlich mechanism is forbidden by the formal selection rules summarized above, which correspond to phonons with exactly zero momentum ($\vec{q} = 0$) [26]. However, when the excitation approaches the band gap energy, a strong LO resonance is observed which is mainly driven by the Fröhlich interaction of free excitons and phonons close to (but not exactly at) the Γ-point, while the less pronounced TO resonance is due to interaction with continuum electron-hole states via the optical deformation potential (ODP) [27].

For polycrystals, the Raman mode frequencies may depend on growth conditions affecting the sample crystalline quality, orientation and size of the crystallites. They are typically located around the following values: A_1(TO) ≅380 cm^{-1}, A_1(LO) ≅574 cm^{-1}, E_1(TO) ≅ 407 cm^{-1}, E_1(LO) ≅583 cm^{-1}, E_2^{low}≅100 cm^{-1} and E_2^{high}≅438 cm^{-1}. Moreover, possible relaxation of the Raman selection rules can be caused by disorder, creating some “forbidden” modes in the Raman spectra. The frequency of the B_1 (low and high) silent modes has been calculated as 260 cm^{-1} and 540 cm^{-1} [28] or 260 cm^{-1} and 552 cm^{-1} [29], respectively.

Figure 2(a) aims to compare measured Raman spectra of two undoped ZnO samples, a molecular beam epitaxy (MBE) grown sample and a thin film deposited by RF-

sputtering. Vertical dashed lines are located at 438 cm^{-1}, 574 cm^{-1} and 583 cm^{-1}, the positions of the main Raman-active modes of ZnO. The main difference between these two Raman spectra is observed in the range of the A_1(LO) and E_1(LO) phonon modes (570 cm^{-1} to 590 cm^{-1}), where abroad band appears only in the spectrum of the sputtered sample. For backscattering from a (001) crystal plane, only E_2 and A_1(LO) modes are allowed by the symmetry selection rules [30].This holds for the MBE-grown sample, except that (i) there is a mode centered at 330cm^{-1} and (ii) the A_1(LO) mode appears too weak. The prominent feature at 330cm^{-1} probably corresponds to the second-order scattering ($E_2^{high} - E_2^{low}$) [27, 30] and has been observed for both single crystal and polycrystalline samples in various configurations [26-31]. The low intensity of the allowed A_1(LO) has also been reported and attributed to the "destructive interference" between the Fröhlich and ODP mechanisms (i.e. a partial cancellation of the matrix elements corresponding to these two mechanisms of electron-phonon coupling) [32, 33].

Figure 2(b) shows the measured Raman spectrum of the sputtered ZnO thin film fitted with ten Lorentzian curves. Besides the already mentioned difference in the region of the A_1(LO) and E_1(LO) phonon modes (broa d band in the 570 cm^{-1} - 590 cm^{-1} range) some smaller features are also revealed by the fitting. Among these the TO-type phonon modes (A_1 at 381 cm^{-1} and E_1 at 407 cm^{-1} [32]) are identified. Their presence in the spectra can be understood by random orientation of the crystallites in the film, since these modes can be allowed for certain scattering configurations. However, the major cause of the clear relaxation of the $\vec{q} = 0$ selection rule, verified in the spectrum of the RF-sputtering grown films is probably caused by crystal lattice disorder due to intrinsic defects. This is also the likely reason for the large enhancement of the LO-phonon-related scattering (the 570 - 590 cm^{-1} band). It may be due to the "forbidden" Fröhlich interaction which becomes overwhelming under resonance conditions as have been shown before for similar samples [17]. Here, far from interband resonance, it can be enhanced by the presence of defects [33, 34]. In the impurity-induced process, the momentum conservation is relaxed and phonons with q vectors away from the Γ point can participate in the Raman scattering.

The larger vectors greatly enhance the Fröhlich contribution, which is known as Gogolin-Rashba mechanism [34]. The enhancing of the Fröhlich mechanism of Raman scattering, can also be associated to phonon confinement in nanocrystalline grains as

reported for quantum dots (QDs) [35], however, this effect is unlikely to be important in these samples, since most of the grains are considerably larger than typical QDs.

As shown in Fig. 2-b) in ZnO(sp) sample the TO and LO-type bands, allowed by crystal lattice disorder, are localized around 380-407 cm^{-1} and 573-582 cm^{-1} respectively. These frequencies may slightly change with the orientation of the crystallite c-axis in respect to the $\vec{q}$ vector. Three other contributions (557 cm^{-1}, 613 cm^{-1} and 663 cm^{-1}) are necessary to fit the spectrum. These contributions have been observed before (see Table 2) but their assignment is not unanimous.

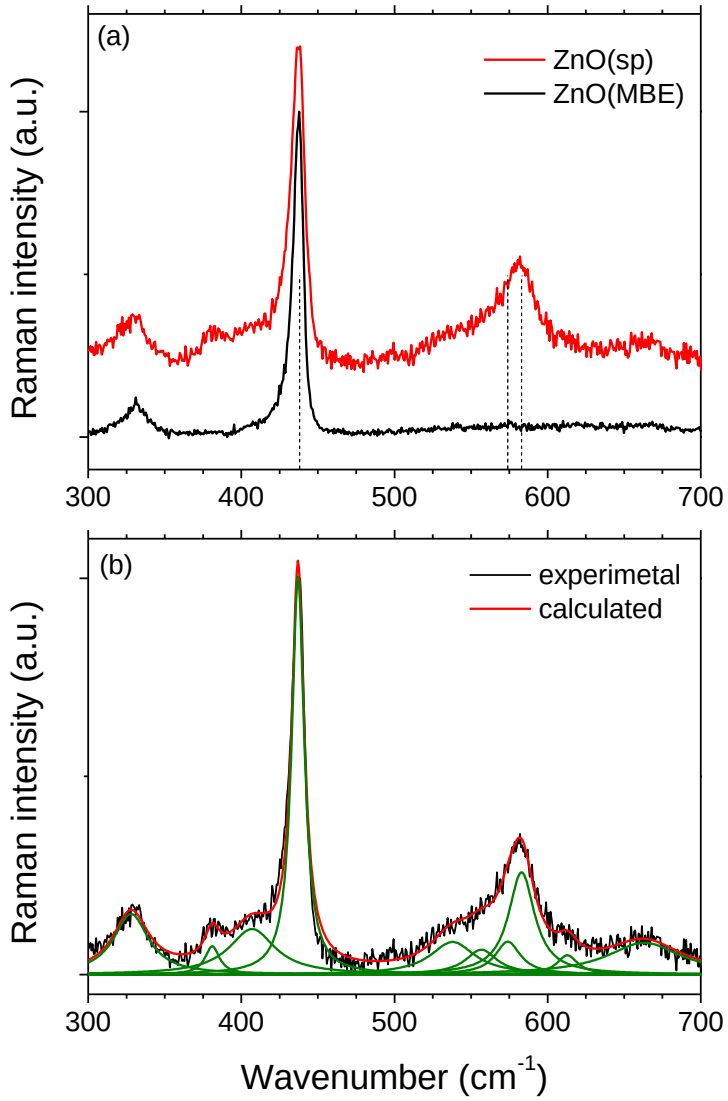

Figure 2. *a) Raman spectra of two ZnO samples, one grown by MBE and the other by RF-sputtering. Dashed vertical lines in this and subsequent figures are at 438 cm^{-1}, 574 cm^{-1} and 583 cm^{-1} corresponding to the E_2^{high}; $A_1(LO)$ and $E_1(LO)$ modes respectively. b) Experimental Raman spectra of the ZnO(sp) film and corresponding fit (red curve). Also shown the ten Lorentzians used for the fit, centered at 328 cm^{-1},*

381 cm^{-1}, 407 cm^{-1}, 437 cm^{-1}, 538 cm^{-1}, 574 cm^{-1}, 583 cm^{-1}, 557 cm^{-1}, 613 cm^{-1}, 663 cm^{-1}.

***Table 2** - Characteristic phonon modes observed in the spectra*

Raman shift (cm^{-1}) (this work)	Raman shift (cm^{-1}) (from literature)	Process	Brillouin zone points/line
328	330-333 [32]	E_2^{high}–E_2^{low}	Γ
381	380 [27]	A_1(TO)	Γ
407	407 [27]	E_1(TO)	Γ
437	437 [27]	E_2^{high}	Γ
538	526 [39]	$E_2^{high} + E_2^{low}$	Γ
557	552 [31]	B_1^{high}	Γ
574	574 [27]	A_1(LO)	Γ
583	583 [27]	E_1(LO)	Γ
613	618 [32]	TA+A_1(TO)	H, M
663	666 [32]	TA+A_1(LO)	M

3.3.2 – ZnO:Al samples

Raman spectra of two ZnO:Al (≈ 0.5 at.%) samples, one doped by co-sputtering, ZnO:Al(sp), and the other by implantation, ZnO:Al(imp), are shown in Figure 3. The spectrum of the ZnO(sp) sample is also shown for comparison. As expected, the inclusion of a dopant, independently of the doping method used, deteriorates the ZnO crystalline lattice as seen in Figure 3 by the strong reduction observed in the intensity of the E_2^{high} mode. We observe no new spectral features that could be associated with Al atoms, in agreement with a previous report on Raman scattering in this material [36].

The relevant ZnO Raman features remain for both types of doping and the peak position of the 438cm^{-1}non-polar mode (E_2^{high}) keeps constant giving the indication of absence of strain in the ZnO lattice at least for this amount of Al. However the intensity ratio between this mode and the polar longitudinal modes in the region 560-590 cm^{-1} decrease in both samples, more in implanted one than in co-sputtered. Also the 330 cm^{-1} multi-phonon mode, present in the non-doped samples, is not observed in the doped samples.

It is observed that, in the LO phonon range, the already characterized bands become broader and peaks positions are slightly changed. The fitting results indicate a red shift for the Al-implanted sample and a small blue shift for the sputtered one, as compared to the undoped ZnO sample. Even when Al content increases to 1 at.%, the blue shift is identical. Therefore, this effect cannot be attributed to LO phonon coupling to plasmons in heavily *n*-type doped samples as observed for some other materials [30], probably because the plasmons are overdamped. Moreover, we cannot attribute these small shifts to strain because there is no such effect for the E_2^{high} mode as discussed above. Most likely the influence of the Al doping on the polar phonon modes occurs through the electronic system but further investigation is necessary. Finally, a decrease in the ratio E_2^{high}/LO, associated with an increase in the full width at half-maximum (FWHM) of the 438 cm^{-1} mode is seen, revealing the decrease in crystalline quality (spectrum not shown).

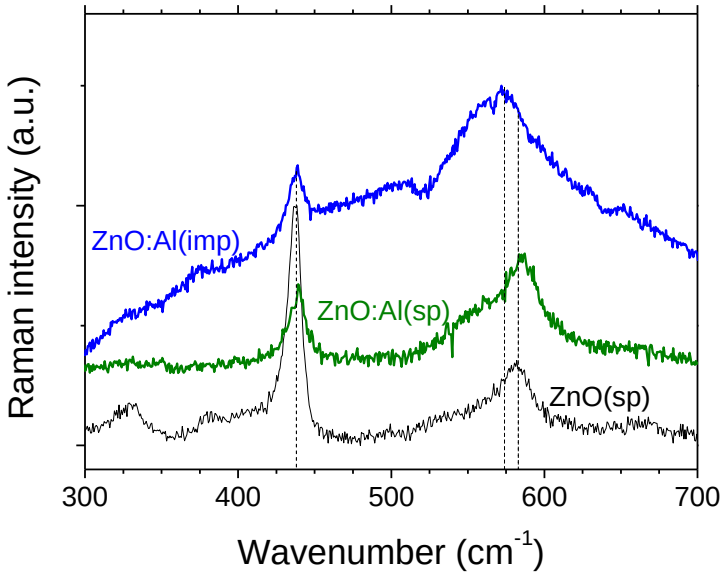

Figure 3. *Raman spectra of ZnO thin films doped with Al (≅0.5 at.%) by co-sputtering and by ion implantation. The Raman spectrum of the pure ZnO thin film (black curve) is also shown for comparison.*

3.3.3 – ZnO:Mn samples

Figure 4 depicts the Raman spectra of ZnO thin films doped with Mn. In part (a) the effect of the doping method, ion implantation and co-sputtering (Mn content ≈1.1 at.%) is illustrated. In parts (b) and (c) the dose effect is shown for both methods. Independently of the doping method the characteristic ZnO E_2^{high}mode is present but, in the 500-

600cm^{-1} range, a considerable difference regarding to pure ZnO and ZnO:Al is seen. In this region the LO band (A_1+E_1) remains but a new strong contribution, around 520-530 cm^{-1}, appears.

The effect of Mn doping on the Raman spectra of ZnO has been widely discussed in the literature [37-44] but the assignment of the new Mn-related features observed is neither unique nor consensual. Yet, some general conclusions can be drawn from these studies. First, the broad band at 520-530 cm^{-1} is specific of Mn doping and has not been observed for other impurities incorporated into ZnO, studied in these works, such as Ti [38], Co [40, 41], Fe and Ni [42]. Secondly, there definitely is a direct correlation between the Mn content and the intensity of this band [39, 40, 43, 44], also observed by us, even though it is not quite linear. Thirdly, this Mn-doping effect is universal with respect to the material preparation methods used. Indeed, it is observed in our ZnO films grown by sputtering and doped by either implantation or co-sputtering, and has also been reported for ZnO:Mn bulk crystals [38] and thin films produced using other growth methods, such as MOCVD [39] or ion implantation [40].

Since Mn atoms are lighter than Zn atoms and certainly substitute the latter in the cationic sublattice of the ZnO crystal, at least partially [23], the most natural explanation for the 520-530 cm^{-1} would be to associate it with a local vibrational mode (LVM) of these substitutional atoms. Indeed, it was suggested in Ref. [37] reporting the first (as far as we know) observation of this band and discussed as plausible by other authors [38, 39, 41, 43]. However, the lack of supporting computational results and some peculiarities in the experimental data related to this band, namely, the non-linear dependence of its intensity upon the Mn concentration and its “fine structure” consisting of two modes resolved in some of the studies [38, 40, 41] (particularly clear in the spectra of bulk ZnO:Mn crystals [38]) caused some doubts among the researchers and speculations about possible alternative explanations.

Structural disorder introduced by the incorporation of manganese can activate the silent modes of ZnO. Using *ab initio* calculations, Serrano *et al.* [29] predicted that the B_1^{low} and the B_1^{high} silent modes of wurtzite ZnO occur at 261 and 552 cm^{-1}, respectively, so the contribution in the region of 520-530 cm^{-1} eventually could be attributed to a disorder activated $2B_1^{low}$ mode, as suggested by the authors of Ref. [40] for one of the additional spectral features introduced by the Mn doping (while the other one, at 520 cm^{-1} still could be related to a local vibration mode.

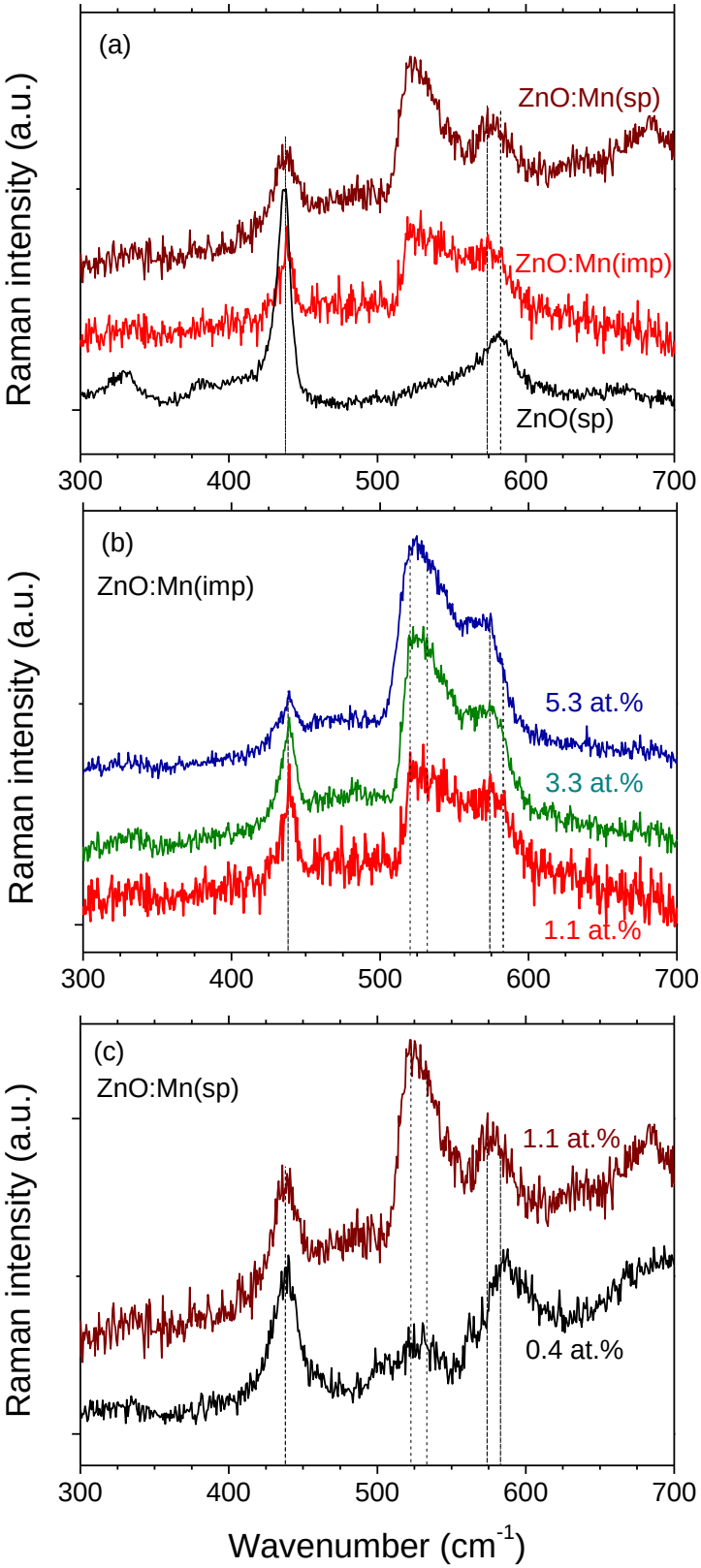

Figure 4. *a) Raman spectra of ZnO thin films doped with Mn (≅1.1 at.%) by co-sputtering and by ion implantation. The Raman spectrum of the pure ZnO film is also shown (black curve). b) Raman spectra of ZnO:Mn thin films doped by ion implantation for different Mn contents. c) Raman spectra of ZnO:Mn thin films doped by co-sputtering for two different Mn contents.*

The possibility that manganese oxides can be responsible for some Raman peaks has also been considered in the literature [44]. Raman peaks of Mn_2O_3 have been found to occur at approximately 525 and 645 cm^{-1} but the intensity of the 645cm^{-1} mode is much stronger than the 525 cm^{-1} one [45], moving away this assumption in our samples. Since no extra peaks were detected on the XRD spectra, it also seems to refute the presence of Mn_2O_3 in these samples. Our opinion concerning the nature of the Mn related 520-530 cm^{-1} Raman band and supporting arguments are presented in Sec. 3.4.

In Figures 4(b) and 4(c) it is possible to observe a decrease in the intensity of the E_2^{high} mode with respect to the modes in the 500-600 cm^{-1} range as the Mn dose increases, in either sputtered or implanted samples. This effect, already noticed for Al doping, is possibly due to an increase in the ZnO lattice damage, however, alloy disorder itself (without radiation damage) can also introduce broadening and shift of Raman modes [40] as has been observed for sol-gel derived ZnO:Mn nanoparticles [46]. As also observed for the ZnO:Al doped samples in the LO phonon range (540-590 cm^{-1}), the multi-Lorentzian fit of the Raman spectra reveals a red shift in the implanted samples as compared to the sputtered ones. This can be related to relaxed crystal vibration modes due to the large number of point defects present.

3.3.4 – ZnO:Mn:Al samples

ZnO samples doped simultaneously with Al and Mn by co-sputtering are transparent but non-conductive (Table 1, sample #11). On the other hand, when Mn doping is achieved by ion implantation on previously conductive ZnO:Al co-sputtered samples (Table 1, samples #9 and #10), the films remain conductive. Possibly it is just a compensation effect, which is only partial in the latter case.

In Fig 5(a) it can be seen the effect of Mn ion implantation on the Raman spectra of the ZnO:Al(sp). As the Mn concentration increases, the 438 cm^{-1} ZnO characteristic Raman peak becomes less important indicating that the crystalline quality of the ZnO lattice is deteriorated. This effect is accompanied by a considerable increase of the intensity of the modes located in the 520-580 cm^{-1} region.

As expected, the 520-530 cm^{-1} mode is only observed in samples with Mn and increases with the increase of Mn content. In the 550-580 cm^{-1} range, the usual effect associated with the doping by ion implantation can be seen – the contributions in this region, whose importance increases with the increase in dopant concentration, shift to lower wavenumbers. Nonetheless, even with high levels of doping, the main Raman features

of the ZnO lattice persist, which manifests that the films remain poly-crystalline and, concomitantly, conductive. In contrast, whenever the magnetic dopant is co-sputtered simultaneously with the Zn and Al ions, the damage in the ZnO lattice is dramatic, as can be seen from figure 5(b), and the films become non-conducting. However, as shown in the XRD spectrum in the inset of Fig. 5 b), ZnO crystallites still are present.

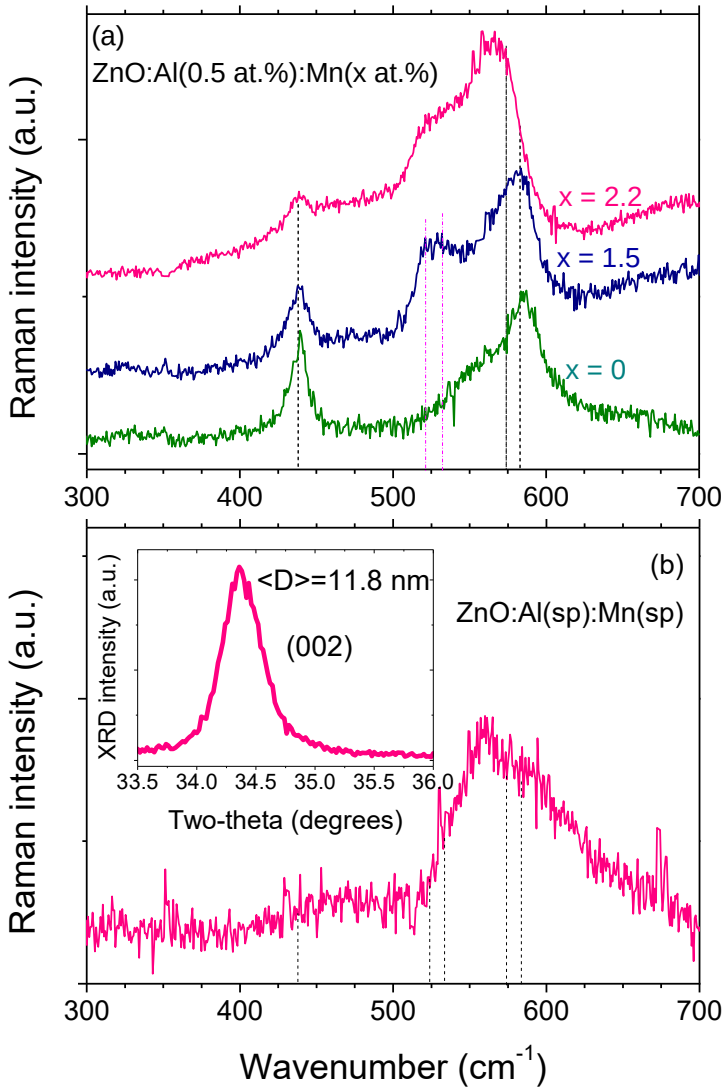

Figure 5. *a) Raman spectra of ZnO:Al(sp):Mn(imp) thin films for two different Mn contents. b) Raman spectra of a ZnO:Al(sp):Mn(sp) sample. The inset shows the XRD pattern of the same sample.*

3.4 Mn related Raman mode

It seems clear from the data and the analysis presented above that the Raman signal in the range of 520-530 cm^{-1} is intrinsically related to the Mn impurity in ZnO lattice. As known, interstitial atoms are weakly linked to the crystal lattice [47] and therefore

cannot vibrate at such a high frequency. The formation of a new phase, such as Mn_2O_3, has been excluded based on the XRD data. Therefore we are forced to assume that Mn atoms substitute Zn in the cationic sublattice of the ZnO crystal, which is not surprising because in many aspects Mn behaves as a usual Group II doping element [23].

We are not aware of published microscopic calculations of the lattice dynamics of ZnO:Mn. However, some simple estimates are possible to make using the available calculated results for pure crystalline ZnO [29, 48] and the lattice dynamics theory for imperfect crystals [49, 50].Assuming that a substituting Mn atom can be modelled as an isotope defect of strength $\varepsilon = 1 - M_{Mn}/M_{Zn}$ (here M_{Mn} and M_{Zn} are atomic masses), the local harmonic vibration frequency can be obtained from the equation:

$$\varepsilon\omega^{*2}\sum_{\sigma}\left|\chi_{\sigma}^{(1)}\right|^2\int\frac{g_{\sigma}\left(\omega'^2\right)}{\omega^{*2}-\omega'^2}d\omega'^2-1=0\,, \tag{1}$$

where σ enumerates branches of the phonon spectrum of the unperturbed crystal, $g_{\sigma}\left(\omega^2\right)$is the density of states (DOS) of the corresponding branch (per unit cell) and $\chi_{\sigma}^{(1)}$ is the vibration eigenvalue amplitude on the sublattice where the impurity atom is (cationic, in our case). For any optical phonon branch it can be estimated as $\left|\chi_{\sigma}^{(1)}\right|^2 = 1/\left(1+M_{Zn}/M_O\right)$, where M_O is the atomic mass of oxygen, since the eigenvectors of optical phonons are inversely proportional to the square root of the atomic mass. This estimate is consistent with the data presented in Ref. [29]. Then we can introduce an effective defect strength of the cation isotope defect, $\varepsilon' = \varepsilon\left|\chi^{(1)}\right|^2$, which yields a value of ≈ 0.04 in our case. Equation (1) is a simple generalization of the equation derived in Ref. [49] for a Bravais lattice. In fact, it can be extended to non-isotope defects as far as they introduce only a local change of the interatomic force constants (for electronic systems it would mean that the perturbation potential is very short-range and its Fourier transform is nearly independent of the k-vector). Having this in mind, we shall treat ε' as a fitting parameter.

Equation (1) can be solved by making a simple approximation for the unperturbed densities of states (normalized to unity), e.g. using a Lorentzian function,

$$g_{\sigma}\left(\omega^2\right)=\frac{\nu}{\pi}\frac{\Gamma_{\sigma}\omega_{\sigma}}{\left(\omega^2-\omega_{\sigma}^2\right)^2+\left(\Gamma_{\sigma}\omega_{\sigma}\right)^2}\,, \tag{2}$$

where ω_{σ} is the DOS peak frequency, Γ_{σ} is a parameter describing the width of the phonon band, and ν is a degeneracy factor ($\nu = 2$ for transverse modes). With the

approximation (2), the integral in Eq. (1) is calculated analytically and the equation for ω^{*2} is easily solved.

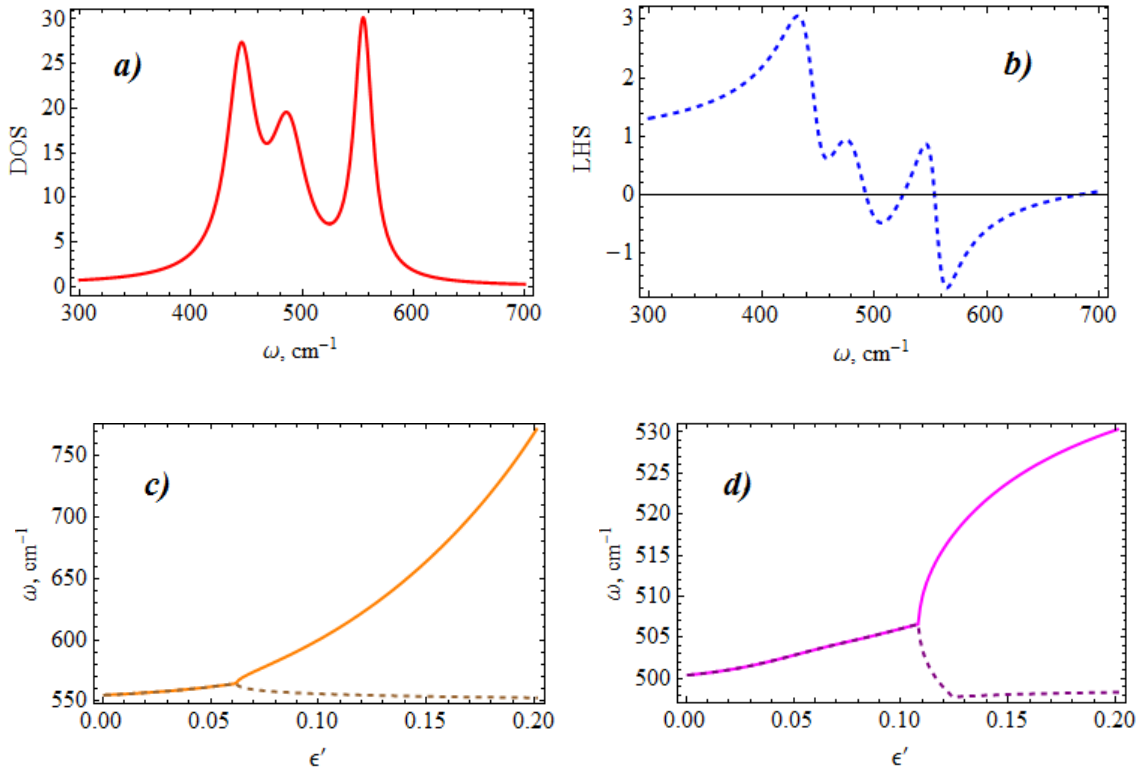

Figure 6. *Density of states in the optical phonon region simulated with three Lorentzians with parameters given in the text (a) and the corresponding spectral dependence of the left hand side (LHS) of Eq. (1) (b); two pairs of solutions of Eq. (1) versus effective defect strength (c and d). Below the bifurcation point two modes originating from the same [LO, plot c), or TO, plot d)] phonon band of ZnO have complex conjugated frequencies.*

By inspecting the calculated DOS data presented in figure 1 of Ref. [29], we can distinguish a TO-type phonon band (400-520 cm^{-1}) and a narrower LO-type band (520-570 cm^{-1}). All other bands can be neglected because they are too far from the interesting frequency range. DOS peaks normally correspond to the Brillouin zone edges where the group velocity vanishes. Taking the values of the phonon frequencies at some high symmetry points [29, 48], we approximated the DOS by three Lorentzians with $\omega_1 \approx$ 450 cm^{-1}, $\Gamma_1 \approx 30$ cm^{-1}, $\omega_2 \approx 490$ cm^{-1}, $\Gamma_2 \approx 40$ cm^{-1}, and $\omega_3 \approx 550$ cm^{-1}, $\Gamma_3 \approx 20$ cm^{-1}; the result is shown in Fig. 6, where the corresponding spectral dependence of the left hand side of Eq. (1) is also presented. Depending on the value of ε', some of the roots can be complex (and come conjugate pairs) and only those with negative imaginary part

of the frequency should be considered as meaningful; they correspond to strongly damped modes. For a certain value of ε', a bifurcation is observed and this is where the local mode appears (e.g. at $\varepsilon'_c \approx 0.05$ in Fig. 6c).

The frequency (ω_l^{LO}) of the lower of the two modes related to the LO band, occurring for $\varepsilon' > \varepsilon'_c$ is found very close to ω_3; the difference does not exceed just few cm^{-1} for any values of the other parameters. Therefore it lies most likely within the continuum of phonon states, it is called resonant and its vibration amplitude behaves as a spherical wave ($\propto \sin(q_0 r)/r$) with a certain wavevector determined by its frequency separation from the band edge. Since this q_0 should not be small, the contribution of the resonant mode to the Raman scattering must be insignificant. In contrast, if ω^* falls outside the LO band, which is the case of the upper mode in Fig. 6c (ω_h^{LO}), its vibration amplitude decreases exponentially with the distance from the site occupied by the impurity atom. Such a mode is not characterized by any specific $\vec{q}$, while the nearby continuum modes correspond to large phonon wavevectors, close to the edges of the Brillouin zone where phonon's group velocity is close to zero. These large $\vec{q}$ modes are Raman inactive, while the local vibration can contribute to the Raman scattering.

A similar scenario takes place for solutions originating from the TO band (Fig. 6d), although here ε'_c is higher. Importantly, there is a gap between the LO and TO parts of the phonon DOS [29] at approximately 525 cm^{-1} (it is not reproduced by our Lorentzian model where only a minimum appears, Fig. 6a). If the upper of the two modes shown in Fig. 6d, ω_h^{TO}, eventually falls into this gap, it will have similar characteristics to the local mode just discussed above.

If we associate ω_h^{TO} with the Mn-related Raman peak, we have to admit a value of the defect strength parameter $\varepsilon' \approx 0.15$, very large compared to what one might expect considering Mn as an isotope defect in the cationic sublattice of ZnO. However, we notice that the existence of the gap in the phonon DOS is a matter of fact, because the phonon dispersion curves were studied using inelastic neutron scattering and also recalculated in the more recent work by Serrano et al. [48] and their result confirm the existence of the gap, even though its exact position may be slightly different from that presented in the earlier work [29] (unfortunately, the DOS is not presented in Ref. [48]). Our simple model shows the possibility that one of the modes produced by Mn atoms

substituting Zn in the cationic sublattice of the ZnO crystal can fall into the gap that does exist slightly below 530 cm^{-1}. Interestingly, if we take $\varepsilon' = 0.16$, we obtain $\omega_h^{TO} \approx$ 525 cm^{-1} and $\omega_h^{LO} \approx 682$ cm^{-1}. This is close to the frequency of a spectral feature seen in the spectra of sputtered ZnO:Mn samples (see Fig. 4) and therefore can be considered as an additional argument in support of the presented model.

The intensity of the experimentally observed feature grows strongly with the increase of Mn content. According to the theory developed in Ref. [50], at finite concentration of impurity the local mode broadens and develops into a band because of the fluctuating distances between neighboring impurity atoms. The amplitude of the local DOS in the vicinity of ω^*_l increases roughly as the square of the impurity concentration (when the latter is small). This is in qualitative agreement with our experimental observation. Moreover, if the interaction between Mn atoms in the lattice is short-range, so that it decreases strongly if they are not nearest neighbors in the sublattice, the local DOS can have a double-peak structure (shown in Fig. 5 of Ref. [49]), which is analogous to the electronic level splitting into two for a pair of identical atoms. This could explain the double-peak structure of the Mn-induced Raman band resolved for higher crystal quality samples [38, 41].

4 - Conclusions

A detailed Raman spectroscopy study of ZnO thin films produced by RF-sputtering have been performed, focused on the changes introduced by doping with Al and Mn impurities.

For undoped polycrystalline films, a strong LO-phonon band, not seen in the spectrum of crystalline MBE-grown ZnO layer, has been found. The presence of this band can be understood by the enhancement of the “forbidden” Fröhlich -type scattering (Gogolin-Rashba mechanism and eventually phonon confinement, although the estimated average grain size is perhaps too large to make the latter important).

It has been shown that ZnO films doped with Al by either co-sputtering or ion implantation yields strong *n*-type conductivity as demonstrated by the results of the electrical resistivity measurements. Contrary to our expectations, we found no evidence of phonon-plasmon coupling in these rather heavily doped samples, possibly because the plasmons are overdamped. The Raman spectra of these samples are similar for both doping methods and no evidence of improvement of the electrical properties of the

material was detected by using ion implantation. Otherwise, Mn magnetic doping of ZnO films by co-sputtering or by ion implantation results in very resistive samples and the Raman spectra shows the presence of Mn-related modes (520-530 cm^{-1}) whose intensity increases with the increase of Mn content. The nature of this mode was discussed and a simple model and arguments were presented in support of our opinion that this Raman feature originates from local vibrations of Mn atoms and their groups (at higher concentrations), substituting Zn in the cationic sublattice of the ZnO crystal. This mode is Raman active because it falls into the gap of the optical phonon density of states of undoped ZnO crystal.

Furthermore, it was shown that is possible to preserve the conductivity of the samples even when both ions were incorporated into the ZnO lattice. Such was achieved using conductive RF-sputtered ZnO:Al films implanted *a posteriori* with Mn ions. This can be an alternative method for the preparation of conductive and transparent ZnO-based dilute magnetic semiconductors (DMS) films for different applications given that preparing DMS with controlled concentration of free carriers is still a challenge. At present, efforts are being made in order to investigate the magnetic properties of these promising materials.

Acknowledgements

This work was supported by (i) FEDER through the COMPETE Program and by the Portuguese Foundation for Science and Technology (FCT) in the framework of the Strategic Project PEst-C/FIS/UI607/2013; (ii) Karlsruhe Nano Micro Facility (KNMF), a Helmholtz Research Infrastructure at KIT; (iii) European COST Actions MP0901-NanoTP, (iv) European Community as an Integrating Activity 'Support of Public and Industrial Research Using Ion Beam Technology (SPIRIT project) under EC contract no. 227012, and (v) ESF Research Networking Programme PLASMONBIONANOSENSE**.** F. Oliveira wishes to acknowledge the FCT PhD Fellowship SFRH-BD-69843-2010. The authors would like to thank Professor Adrian Kozanecki (Institute of Physics of the Polish Academy of Sciences) for the MBE sample, to Professor David J. Barber (University of Essex) for his critical reading of this manuscript, and to Professor J. Pedro Alpuim (INL) for the possibility of using the Raman WiTec system.

References

[1] - Zhang Xiaodan, Fan Hongbing, Zhao Ying, Sun Jian, Wei Changchun, Zhang Cunshan, *Appl. Surf. Sci.* 253, 3825 (2007)

[2] - T. M. Børseth, J. S. Christensen, K. Maknys, A. Hallén, B. G. Svensson, A. Yu. Kuznetsov, *Superlattices and Microstructures* 38, 464 (2005)

[3] - V. A. Coleman, H. H. Tan, C. Jagadish, S. O. Kucheyev, J. Zou, *Appl. Phys. Lett.* 87, 231912 (2005)

[4] - J. G. Lu, Z. Z. Ye, Y. J. Zeng, L. P. Zhu, L. Wang, J. Yuan, B. H. Zhao, Q. L. Liang, *J. Appl. Phys.* 100, 073714 (2006)

[5] - M. Jin, J. Feng, Z. De-heng, M. Hong-lei, L. Shu-ying, *Thin Solid Films* 357, 98 (1999)

[6] - H. Ohno, *Science* 281, 951 (1998)

[7] - S. A. Wolf, D. D. Awschalom, R. A. Buhrman, J. M. Daughton, S. von Molnar, M. L. Roukes, A. Y. Chtchelkanova, D. M. Treger, *Science* 294, 1488 (2001)

[8] - T. Dietl, H. Ohno, F. Matsukura, J. Cibert, D. Ferrand, *Science* 287, 1019 (2000)

[9] - T. Dietl, H. Ohno, F. Matsukura, *Phys. Rev. B* 63, 195 (2001)

[10] - K. Sato, H. Katayama-Yoshida, *Jpn. J. Appl. Phys.* 39, L555 (2000)

[11] - T. Fukumara, Z. Jin, M. Kawasaki, T. Shono, T. Hasegawa, S. Koshihara, H. Koinuma, *Appl. Phys. Lett.* 78, 958 (2001)

[12] - S. W. Jung, S. J. An, Gyu-Chui Yi, C. U. Jung, Sung-Ik Lee, Suglae Cho, *Appl. Phys. Lett.* 80, 4561 (2002)

[13] - M. Bouloudenine, S. Colis, N. Viart, A. Dinia, *Chem. Phys. Lett.* 397, 73 (2004)

[14] - J. Alaria, P. Turek, M. Bernard, M. Bouloudenine, A. Berbadj, N. Brihi, G. Schmerber, S. Colis, and A. Dinia, *Chem. Phys. Lett.* 415, 337 (2005)

[15] - Yao-Ming Hao, Shi-Yun Lou, Shao-Min Zhou, Rui-Jian Yuan, Gong-Yu Zhu, and Ning Li, *Nanoscale Res. Lett.* 7, 100 (2012)

[16] - N. H. Hong, T. Sakai; V. Brizé, *J. Phys: Condensed Matter* 19, 036219 (2007)

[17] - M. F. Cerqueira, M. I. Vasilevskiy, F. Oliveira, A. G. Rolo, T. Viseu, J. Ayres de Campos, E. Alves, R. Correia, *J. Phys: Condensed Matter* 23, 334205 (2011)

[18] - Stopping and Range of Ions in Matter, www.srim.org

[19] - D. A. Minkov, *J. Phys D: Appl. Phys*. 22, 199 (1989)

[20] - M. Bououdina, K. Omri, M. El-Hilo, A. El Amiri, O. M. Lemine, A. Alyamani, E.K. Hlil, H. Lassri, L. El Mir, *Physica E* 56, 107 (2014)

[21] – Sharda, K. Jayanthi, S. Chawla, *Applied Surface Science* 256, 2630 (2010)

[22] - T. H. de Keijser, J. I. Langford, E. F. Mittemeyer, A. B. P. Rogels*, J. Appl. Crystallogr.* 11, 10 (1978)

[23] - C. Klingshirn, J. Fallert, H. Zhou, J. Sartor, C. Thiele, F. Maler-Flaig, D. Schneider, and H. Kalt, *Phys. Status Solidi B* 247, 1424 (2010)

[24] - T. C. Damen, S. P. S. Porto, B. Tell, *Phys. Rev.* 142, 570 (1966)

[25] - U**.** Ozgur, Y. I. Alivov, C. Liu, A. Teke, M. A. Reshchikov, S. Dogan, V. Avrutin, S. J. Cho and H. Morkoc**,** ***J. Appl. Phys.*** 98**,** 041301 **(**2005**)**

[26] - H. Zhou, L. Chen, V. Malik, C. Knies, D. M. Hofmann, K.P. Bhatti, S. Chaudhary, P. J. Klar, W. Heimbrodt, C. Klingshirn, H. Kalt, *Phys. Status Solidi* A 204, 112 (2007)

[27] - J. M. Calleja, M. Cardona, *Phys. Rev. B* 16, 3753 (1977)

[28] - F. Decremps, J. Pellicer-Porres, A. Marco Saitta, J.-C. Chervin, A. Polian, *Phys. Rev.* B 65, 092101 (2002)

[29] - J. Serrano, A. H. Romero, F. J. Manjón, R. Lauck, M. Cardona, A. Rubio, *Phys. Rev. B* 69, 094306 (2004)

[30] - R. Cuscó, E. Alarcon-Llado, J. Ibanez, L. Artus, J. Jimenez, B. Wang, M. J. Callahan, *Phys. Rev. B* 75, 165202 (2007)

[31] - M. F. Cerqueira, A. G. Rolo, T. Viseu, J. Ayres de Campos, T. de Lacerda-Arôso, F. Oliveira, M. I. Vasilevskiy, E. Alves, *Phys. Status Solidi C* 7, 2290 (2010)

[32] - U**.** Ozgur, Y. I. Alivov, C. Liu, A. Teke, M. A. Reshchikov, S. Dogan, V. Avrutin, S. J. Cho and H. Morkoc**,** ***J. Appl. Phys.***98**,** 041301 **(**2005**)**

[33] - J. Merendez and M. Cardona, *Phys. Rev. B* 31, 3696 (1985)

[34] - A. A. Gogolin and E.I. Rashba, *Solid State Commun* 19, 1177 (1976)

[35] - A. G. Rolo and M. I. Vasilevskiy, *J. Raman Spectroscopy* 38, 618 (2007)

[36] - A. El Manouni, F. J. Manjón, M. Mollar, B. Maríb, R. Gómez, M. C. López, J. R. Ramos-Barrado*, Superlattices and Microstructures* 39, 185 (2006)

[37] - L. W. Yang, X. L. Wu, G. S. Huang, T. Qiu, Y. M. Yang, *Journal of Applied Physics* 97, 014308 (2005)

[38] - W. Gebicki, K. Osuch, C. Jastrzebski, Z. Golacki, M. Godlewski, *Superlattices and Microstructures* 38, 428 (2005)

[39] - J. Gleize, E. Chikoidze, Y. Dumont, E. Rzepka, O. Gorochov*, Superlattices and Microstructures* 42, 242 (2007)

[40] - M. Schumm, M. Koerdel, S. Müller, H. Zutz, C. Ronning, J. Stehr, D M Hofmann, J. Geurts, *New Journal of Physics* 10, 043004 (2008)

[41] - M. Jouanne, J. F. Morhange, W. Szuszkiewicz, Z. Gołacki, A. Mycielski, *Phys. Status Solidi* C 3, 1205 (2006)

[42] - M. Schumm, M. Koerdel, S. Müller, C. Ronning, E. Dynowska, Z. Gołacki, W. Szuszkiewicz, J. Geurts, *Journal of Applied Physics* 105, 083525 (2009)

[43] - X. Teng, W. Yu, L. Z. Y. Wu, W. Gao, G. Fu, In: *Proc. International Conference on Electronics and Optoelectronics* (ICEOE 2011), Vol 3, pp. V3-195-V3-198 (2011)

[44] - Y. M. Hu, C. Y. Wang, S. S. Lee, T. C. Han, W. Y. Chou, G. J. Chen, *J. Raman Spectroscopy* 42, 434 (2011)

[45] - M. A. García, M. L. Ruiz-González, A. Quesada, J. L. Costa-Kramer, J. F. Fernández, S. J. Khatib, A. Wennberg, A. C. Caballero, M. S. Martín-González, M. Villegas, F. Briones, J. M. González-Calbet, A. Hernando, *Phys. Rev. Lett.* 94, 217206 (2005)

[46] - J. B. Wang, H. M. Zhong, Z. F. Li, Wei Lu, *Journal of Applied Physics* 97, 086105 (2005)

[47] - A. A. Maradudin, E. W. Montroll, and G. H. Weiss, *Theory of lattice dynamics in the harmonic approximation,* Academic Press, N-Y (1963)

[48] - J. Serrano, F. J. Manjón, A. H. Romero, A. Ivanov, M. Cardona, R. Lauck, A. Bosak and M. Krisch, *Phys. Rev. B* 81, 174304 (2010)

[49] - I. M. Lifshitz, *Nuovo Cimento*, Supplemento A1, Vol. III, Ser. X, p. 716 (1956)

[50] - I. M. Lifshitz, *Physics - Uspekhi* 7, 549 (1965)